Electronic Supplementary Material (ESI) for ChemComm.

Integrating single Co sites into highly crystalline covalent triazine frameworks for photoreduction of CO_2

Xunliang Hu,[a] Lirong Zheng,[b] Shengyao Wang,[c] Xiaoyan Wang*[a] and Bien Tan*[a]

a. Key Laboratory of Material Chemistry for Energy Conversion and Storage Ministry of Education, Hubei Key Laboratory of Material Chemistry and Service Failure, School of Chemistry and Chemical Engineering, Huazhong University of Science and Technology, Luoyu Road No. 1037, 430074 Wuhan, P. R. China.
b. Beijing Synchrotron Radiation Facility, Institute of High Energy Physics, Chinese Academy of Sciences, Beijing 100049, P. R. China
c. College of Science, Huazhong Agricultural University, Wuhan, 430070, P. R. China

E-mail: **xiaoyan_wang@hust.edu.cn**

E-mail: **bien.tan@mail.hust.edu.cn**

1. Materials and methods

All reagents were obtained from Aladdin. All chemicals were used without further purification.

1.1 Solution nuclear magnetic resonance

^{1}H NMR spectra were recorded in solution at 600 MHz, using a Bruker Avance 600 NMR spectrometer.

1.2 Fourier-transform infrared spectroscopy

The formation of triazine unit was confirmed by Fourier-transformed infrared (FT-IR) spectra in ATR mode with a Bruker Vertex 70 FT-IR spectrometer.

1.3 Powder X-ray diffraction

Powder X-ray diffraction (PXRD) data were collected by a Smart X-ray diffractometer (Smartlab SE, Rigaku, Japan) with Cu Kα radiation (λ = 1.54178 Å). Films were ground to powders and mounted as integral films onto a silicon zero background holder. The PXRD patterns were recorded from 3 to 45° (2θ) with a step size of 0.02° and a scan rate of 5° per minute.

1.4 Gas sorption analysis

Apparent surface areas were measured by nitrogen sorption at 77.3 K using a Micromeritics ASAP 2460 volumetric adsorption analyzer. Powder samples were degassed offline at 393 K for 12 h under dynamic vacuum (10^{-5} bar) before analysis. Pore size distributions of CTFs from fitting the nonlocal density functional theory (NL-DFT) model to the adsorption data. Carbon dioxide isotherms were collected up to a pressure of 1 bar on a Micromeritics ASAP2020 at 273 and 298 K.

1.5 Solid-state ^{13}C CP/MAS NMR spectroscopy

Solid-state ^{13}C CP/MAS NMR spectroscopy using a WB 400 MHz Bruker Avance II spectrometer with the contact time of 2 ms (ramp 100) and pulse delay of 3 s.

1.6 Thermogravimetric analysis

Thermogravimetric analysis was performed on an Pyris1 TGA by heating samples at 10 °C min^{-1} under nitrogen in open Pt pans to 650 °C.

1.7 UV-Visible absorption spectra

UV-Visible absorption spectra of the polymers were measured on a Shimadzu UV-

2600 UV-Vis spectrometer by measuring the reflectance of powders in the solid state.

1.8 Scanning electron microscopy

Imaging was performed using a FEI Sirion 200 field emission scanning electron microscope (FE-SEM).

1.9 Transmission electron microscopy

HAADF-STEM images were obtained on a Tecnai G2 F30, FEI Holland microscope at an accelerating voltage of 200 kV. The samples were prepared by drop-casting sonicated ethanol suspensions of the materials onto a copper grid.

1.10 X-Ray photoelectron spectroscopy measurements

X-ray photoelectron spectroscopy (XPS) were carried out on an Axis Ultra DLD 600 W instrument (Shimadzu, Japan).

1.11 X-Ray absorption fine structure spectra measurements and Analysis

The X-ray absorption find structure spectra (Co K-edge) were collected at 1W1B station in Beijing Synchrotron Radiation Facility (BSRF). The storage rings of BSRF was operated at 2.5 GeV with a maximum current of 250 mA. Using Si (111) double-crystal monochromator, the data collection were carried out in transmission mode using ionization chamber. All spectra were collected in ambient conditions.

The acquired EXAFS data were processed according to the standard procedures using the ATHENA module implemented in the IFEFFIT software packages. The k^3-weighted EXAFS spectra were obtained by subtracting the post-edge background from the overall absorption and then normalizing with respect to the edge-jump step. Subsequently, k^3-weighted $\chi(k)$ data of Co K-edge were Fourier transformed to real (R) space using a hanning windows (dk = 1.0 $Å^{-1}$) to separate the EXAFS contributions from different coordination shells. To obtain the quantitative structural parameters around central atoms, least-squares curve parameter fitting was performed using the ARTEMIS module of IFEFFIT software packages.

1.12 Isotope–labelling experiment

Isotope–labelling experiment for CO_2 reduction was performed using CTF-Bpy-Co powder (10 mg), 2,2'-bipyridyl (15 mg), acetonitrile, water and triethanolamine (3:1:1 vol. mixture, 5 mL) and sealed with a septum. The resulting suspension was

ultrasonicated for 5 minutes and then purged with $^{13}CO_2$ for 5 minutes. The reaction mixture was illuminated with a 300 W Xe light source equipped with a $\lambda > 420$ nm cut-off filter. The gas-phase was analyzed by using a gas chromatography (Agilent GC-MS 7890B) with a mass-spectrometer (Agilent GC-MS 5977B) equipped with a GC-CARBONPLOT column (60 m length, 0.32 mm inner diameter).

Synthesis of CTF-Bpy. A flask was charged with [2, 2' - Bipyridine] - 5, 5'-dicarboximidamide hydrochloride (153 mg, 0.5 mmol), Cs_2CO_3 (0.245 g, 0.75 mmol), 1, 2-dichlorobenzene (5 mL), DMSO (5 mL), this mixture was heated to 100 ^oC with stirring. 2, 2'-bipyridyl - 5, 5'- dialdehyde (56 mg, 0.25 mmol) was dissolved in 1, 2-dichlorobenzene (5 mL) and DMSO (5 mL). Added the solution of 2, 2'-bipyridyl - 5, 5'- dialdehyde into [2, 2'- Bipyridine] - 5, 5'-dicarboximidamide hydrochloride solution by peristaltic pump with 20 μL min^{-1}. Heated the mixture at 100 ^oC for 24 h, then 180 ^oC for 48 h. Filter the yellow precipitate and washed it with N, N-dimethylformamide (100 mL), and deionized water (200 mL). After freeze drying, the product was obtained as yellow powder (145 mg, 92 %). Anal. Calcd for $(C_{12}H_{10}N_4)_n$: C, 68.56; H, 4.79; N, 26.65. Found: C, 52.94; H, 4.79; N, 17.03.

Cobalt Loading onto CTFs. Mixed CTF-Bpy (20 mg) with $CoCl_2 \cdot 6H_2O$ (9 mg) in acetonitrile (20 mL), and the resulting suspension was ultrasonicated for 6 h at room temperature. Then filtered the solid and washed it with acetonitrile (200 mL). Dried under vacuum at 60 °C overnight to yield CTF-Bpy-Co. The cobalt content was determined by inductively coupled plasma-optical emission spectrometry to be 1.4 wt %.

Carbon Dioxide Reduction Experiments. A quartz flask was charged with the CTF-Bpy-Co powder (10 mg), 2,2′-bipyridyl (15 mg), ($[Ru(Bpy)_3Cl_2]\cdot 6H_2O$, 6.5 mg), acetonitrile, water, and triethanolamine (TEOA) (3:1:1 vol mixture, 20 mL) and sealed. The resulting suspension was ultrasonicated for 5 min and then purged with CO_2 for 15 min. The reaction mixture was illuminated with a 300 W Xe light source (perfect light) equipped with $\lambda > 420$ nm cutoff filter. Gaseous product was acquired with gas-tight syringe and analyzed on Shimadzu GC-2014 gas chromatograph

equipped with ShinCarbon ST micropacked column (Restek 80 - 100 mesh, 2 m length, and 0.53 mm inner diameter) and thermal conductivity detector calibrated against standard gas mixtures of known concentration. Isotope-labeling $^{13}CO_2$ reduction test was performed under the same condition mentioned above andCO_2 was fully replaced by $^{13}CO_2$. The gas product was analyzed by gas chromatography (Agilent 7890B GC) with mass spectrometer (Agilent 5977B MS) equipped with GC-CARBONPLOT column (60 m length, 0.32 mm inner diameter).

2. Synthetic procedures

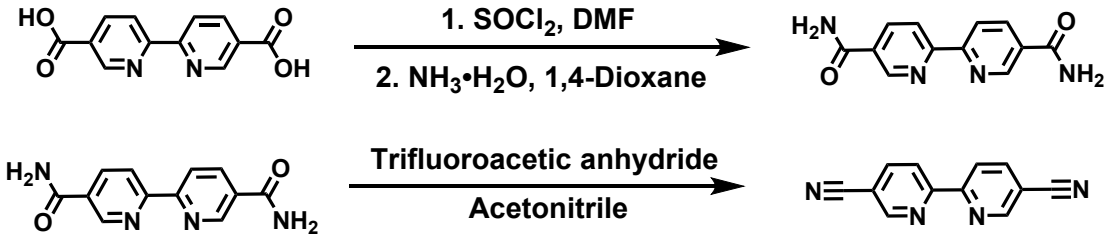

2,2'-bipyridine-5,5'-dicarbonitrile: A 250 mL flask with 2,2'-bipyridine-5,5'-dicarboxylic (8g, 32.8 mmol), added 140 mL $SOCl_2$ and few drops DMF into the flask, then heated at 80 ^oC for 5 h. The $SOCl_2$ was removed by rotary evaporation. The solid was dispersed in 160 mL 1,4-dioxane and added 160 mL ammonia into the flask, this mixture was stirred at 25 ^oC for 24 h. The white precipitate formed was collected and washed with hot ethanol to get 5,5'-dicarboxamide-2,2'-bipyridine. Trifluoroacetic anhydride (17 ml, 121 mmol) was added dropwise to a stirred ice-cooled suspension of 5,5'-dicarboxamide-2,2'-bipyridine (2.1 g, 8.7 mmol) in anhydrous acetonitrile (90 ml) and anhydrous TEA (30 ml). Over the period of the addition, the temperature was kept below 5 °C. The reaction mixture was then allowed to warm to room temperature and stirred for another 24 h. Then 100 ml of distilled water were added to the reaction mixture, the solid product was collected by filtration and washed with water. The ^{1}HNMR shown in Figure S1.

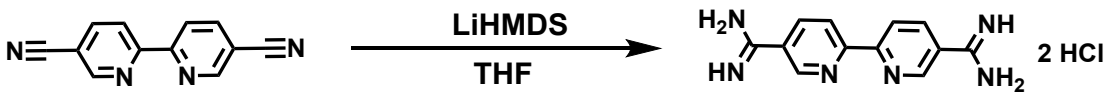

2,2'-bipyridine-5,5'-dicarboximidamide hydrochloride: 2,2'-bipyridine-5,5'-dicarbonitrile (2.06 g, 10 mmol) were dispersed in 20 mL anhydrous THF in a 100

mL flask, the temperature was cooled to 5 °C. 40 mL (1.0 M in THF) Lithium bis(trimethylsilyl)amide was added into the flask. The solution was stirred at 25 °C for 3 h. Then, the solution was acidified by added 5 mL HCl at 5 °C and stay at 25 °C for 12 h. The white solids were collected by filtration and washed with ethanol. The ^{1}HNMR shown in Figure S2.

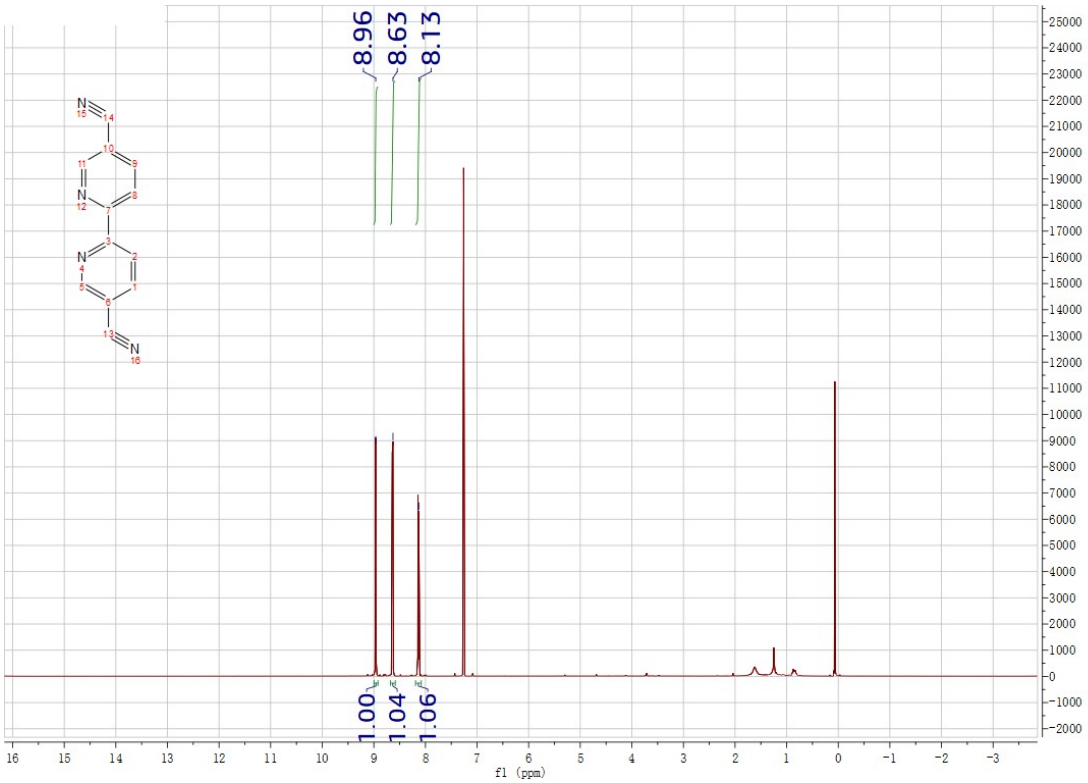

Figure S1. ^{1}H NMR spectrum of 2,2'-bipyridine-5,5'-dicarbonitrile measured in $CDCl_3$.

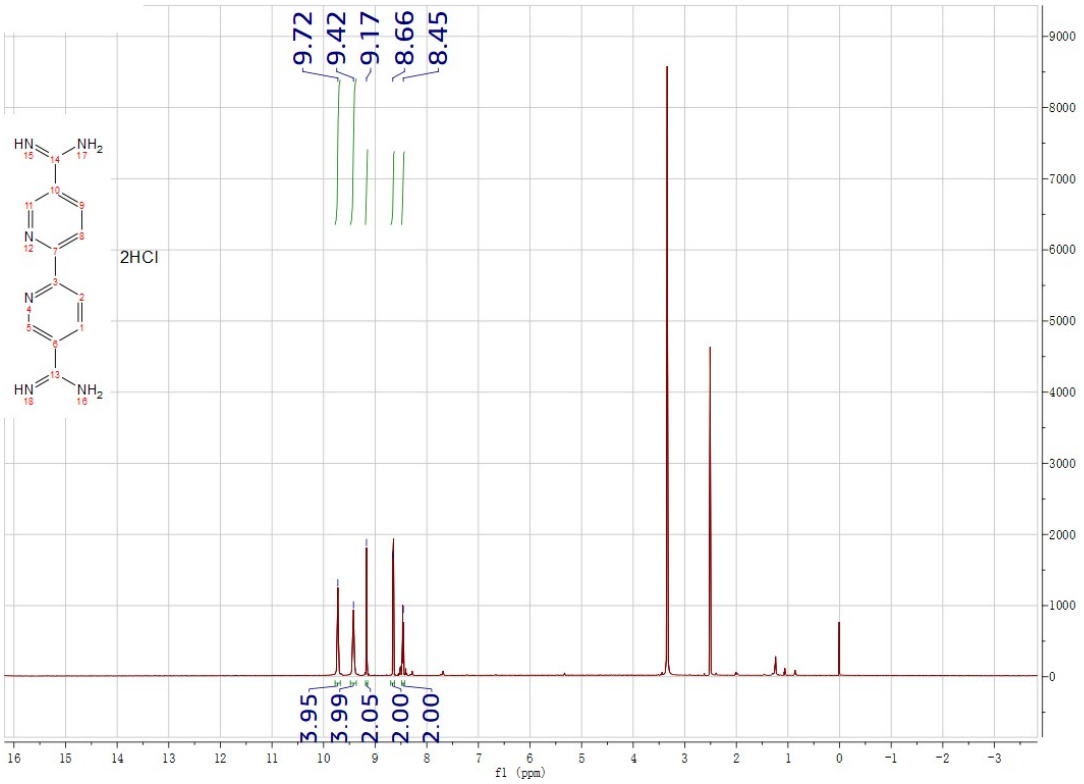

Figure S2. ^{1}H NMR spectrum of 2,2'-bipyridine-5,5'-dicarboximidamide hydrochloride measured in d_6-DMSO.

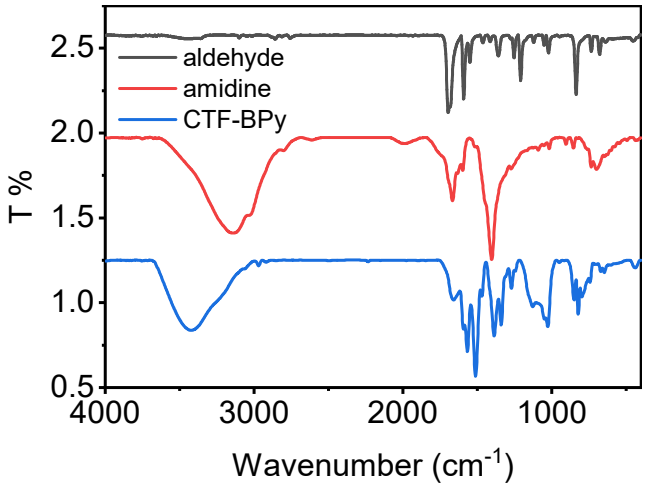

Figure S3. The FTIR of the monomers and CTF-Bpy.

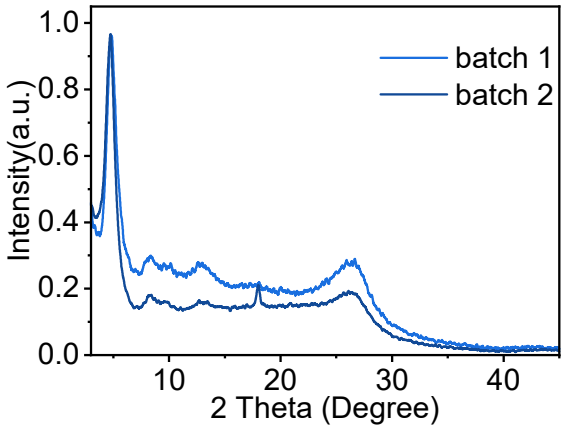

Figure S4. The PXRD curve of CTF-Bpy prepared in different batch.

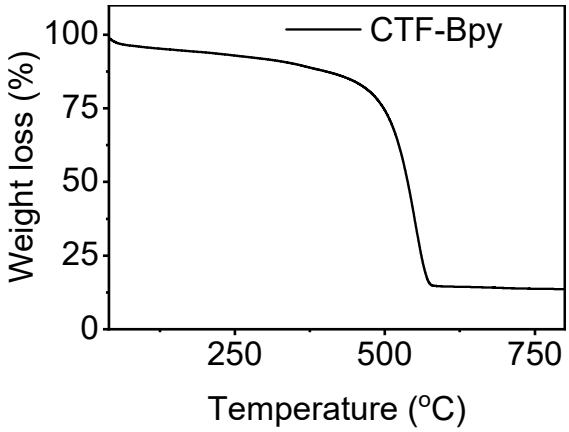

Figure S5. TGA curve of CTF-Bpy.

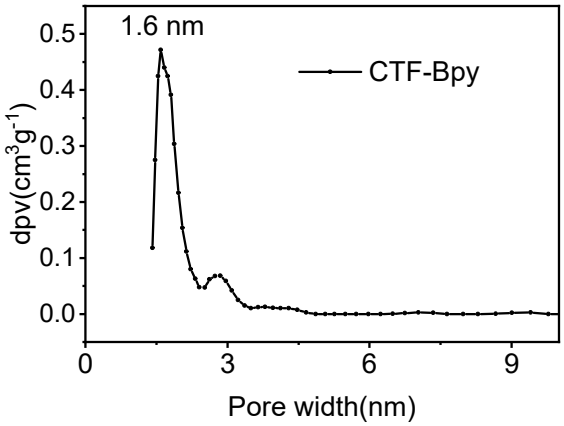

Figure S6. The pore size distribution of CTF-Bpy.

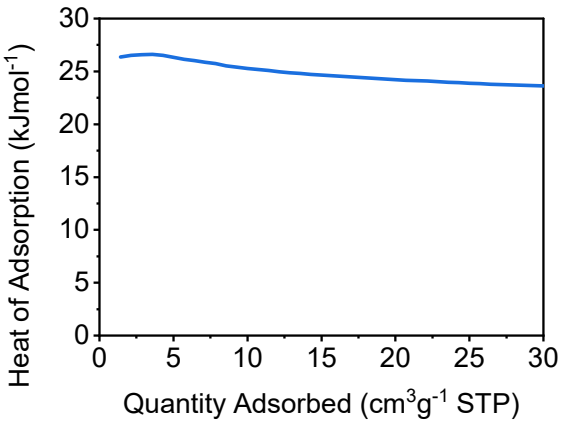

Figure S7. Isosteric heats of adsorption for CO_2 calculated from the adsorption isotherms collected at 273 K and 298 K (CTF-Bpy).

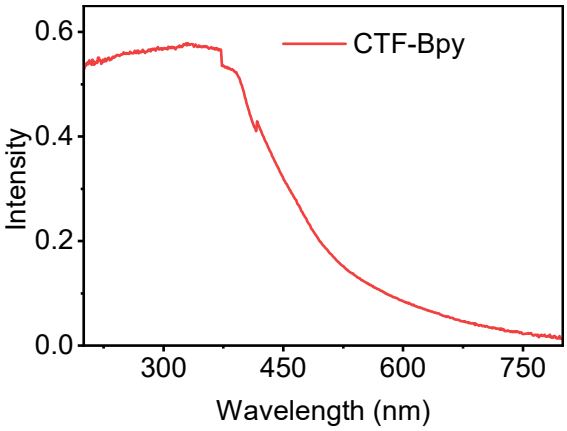

Figure S8. The UV-Vis of the CTF-Bpy.

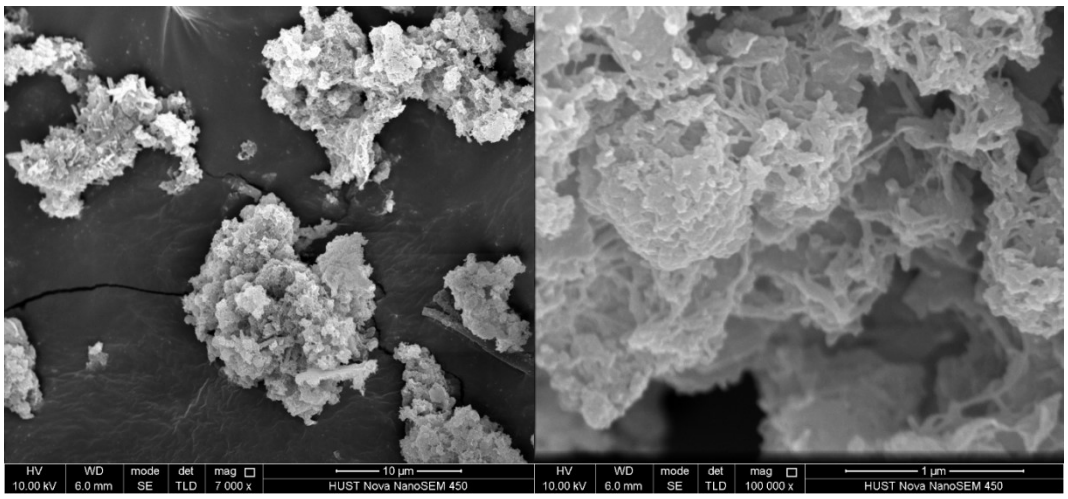

Figure S9. SEM images of CTF-Bpy.

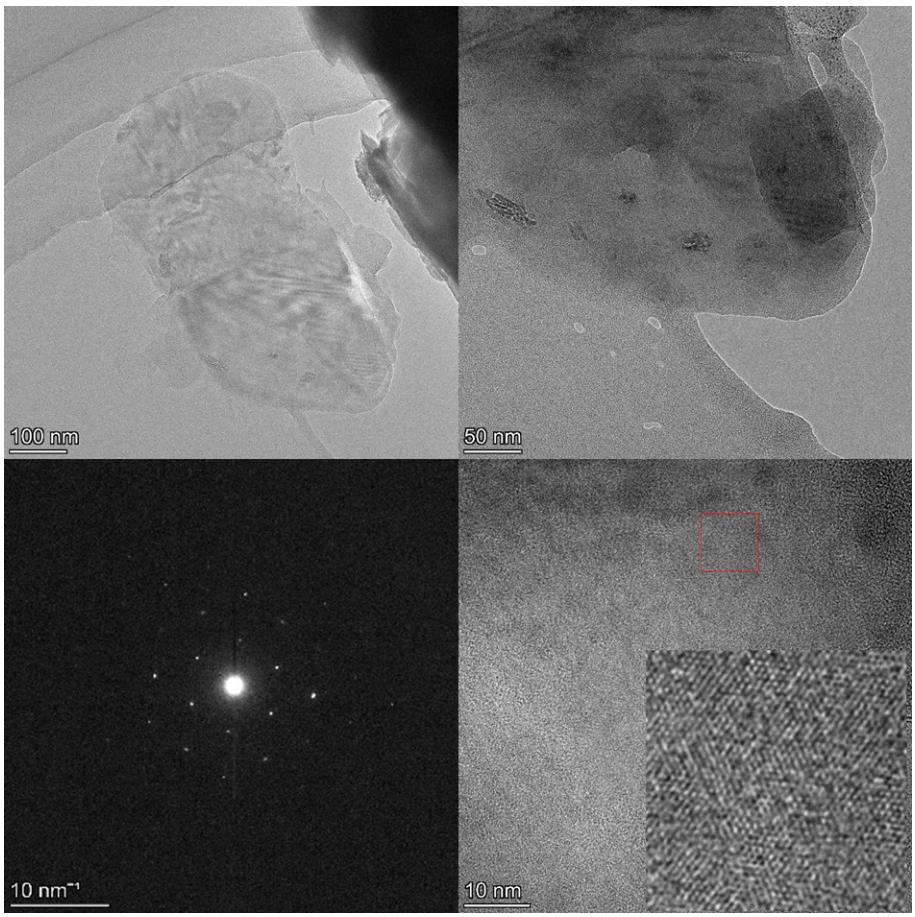

Figure S10. HRTEM images of CTF-Bpy.

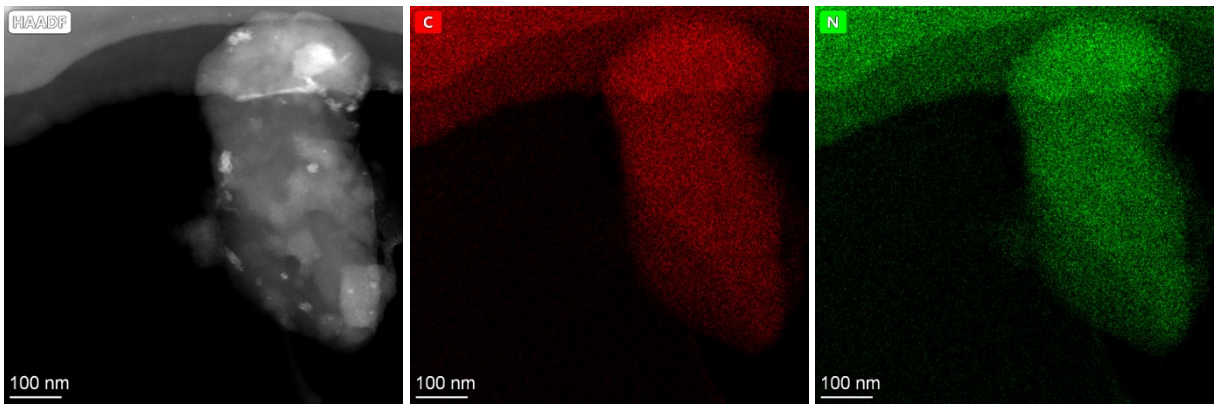

Figure S11. Elemental mapping images of CTF-Bpy.

Table S1. Unit cell parameters of CTF-Bpy.

Simulated Space group : P31m
a/Å = 21.755(5)
c/Å =3.438(2)
α/° = 90.0
β/° = 90.0
γ/° = 120

Table S2. Comparison of $FWHM_{100}$ of reported CTFs and as-synthesized CTF-Bpy.

CTFs	$FWHM_{100}$	Method	Reference
CTF-Bpy	**0.76 °**	**Polycondensation**	**This work**
CTF-HUST-1	Amorphous	Polycondensation	*Angew. Chem. Int. Ed.,* 2017, 56, 14149[1]
CTF-HUST-C1	1.67°	Polycondensation	*Angew. Chem. Int. Ed*., 2018, 57, 11968[2]
CTF-HUST-HC1	1.91°	Polycondensation	*Adv. Mater.*, 2019, 31, 1807865 [3]
CTF-HUST-A1	2.0 ~ 3.0°	Polycondensation	*Angew. Chem. Int. Ed*., 2020, 59, 6007[4]
CTF-HUST-Sx	2.0 ~ 3.0°	Polycondensation	*Chem. Mater.*, 2021, 33 , 1994[5]
CTF-HUST-E1	1.45°	Polycondensation	*J. Mater. Chem. A*, 2021, 9, 16405[6]
CTF-1	0.5~0.8 ° (estimated)	CF_3SO_3H catalyzed	*J. Am. Chem. Soc.*, 2020, 142, 6856[7]
CTF-1	0.44 ~ 0.81°	CF_3SO_3H catalyzed	*Angew. Chem. Int. Ed*., 2022, 61, e202116875[8]
CTF-1	N.A.	Ionothermal	*Angew. Chem. Int. Ed.,* 2022, 61, e202201482[9]

Table S3. Comparison of $FWHM_{100}$ of reported COFs and as-synthesized CTF-Bpy.

COF	FWHM100	Reference
CTF-Bpy	**0.76°**	**This work**
g-$C_{31}N_3$-COF	0.884°	*Nat. Commun.* 2019, 10, 2467[10]
g-$C_{34}N_6$-COF	0.882°	*Angew. Chem. Int. Ed.* 2019, 58, 12065[11]
g-$C_{37}N_3$-COF	0.934°	*Nat. Commun.* 2019, 10, 2467[10]
g-$C_{33}N_3$-COF	0.707°	*J. Am. Chem. Soc.* 2019, 141, 14272[12]
g-$C_{40}N_3$-COF	0.305°	*Nat. Commun.* 2019, 10, 2467[10]
COF-1	0.3°	*Angew. Chem. Int. Ed.* 2019, 58, 13753[13]
COF-p-3Ph	0.317°	*J. Am. Chem. Soc.* 2020, 142, 11893[14]
COF-p-2Ph	0.463°	*J. Am. Chem. Soc.* 2020, 142, 11893[14]
COF-m-3Ph	0.563°	*J. Am. Chem. Soc.* 2020, 142, 11893[14]

Table S4. EXAFS fitting parameters at the Co K-edge for CTF-Bpy-Co.

Sample	Shell	N [a]	R (Å) [b]	σ^2 (Å$^2\cdot10^{-3}$) [c]	ΔE0 (eV) [d]	R factor (%)
sample	Co-N(O)	6.45	2.13	9.1	-1.3	0.1

[a] *N*: coordination numbers; [b] *R*: bond distance; [c] σ^2: Debye-Waller factors; [d] ΔE_0: the inner potential correction. *R* factor: goodness of fit. S_0^2 for Co-N(O) were set as 0.9, which was obtained from the experimental EXAFS fit of CoPc reference by fixing CN as the known crystallographic value and was fixed to all the samples [15-17].

Table S5. Performance comparison of our samples with state-of-the-art COFs and CTFs catalysts for the photocatalytic CO_2 reduction.

Photocatalyst	Main products and highest yield (μmol h^{-1} g^{-1})	Electron donor	Selectivity	Irradiation condition	Reference
CTF-Bpy-Co $[Ru(Bpy)_3]Cl_2$	1200 (CO)	TEOA	83.8 % CO)	λ > 420 nm (300 W Xe Light source)	This work
DQTP-COFCo $[Ru(Bpy)_3]Cl_2$	1020 (CO)	TEOA	59.4%(CO)	λ > 420 nm (300 W Xe Light source)	[18]
Re-Bpy-sp^2c-COF $Ir[dF(CF_3)ppy]_2$ (dtBpy))PF_6	1400(CO)	TEOA	86%(CO)	λ > 420 nm (300 W Xe Light source)	[19]
Ni-TpBpy-COF $[Ru(Bpy)_3]Cl_2$	966 (CO)	TEOA	96%(CO)	λ ≥ 420 nm (300 W Xe	[20]

				light source)	
TTCOF-Zn	2.06 (CO)	H_2O	100%(CO)	800 nm ≥ λ ≥ 420 nm (300 W Xe light source)	[21]
ACOF-1	60 (CH_3OH)	H_2O	-	800 nm ≥ λ ≥ 420 nm (500 W Xe light source)	[22]
N_3-COF	98.3 (CH_3OH)	H_2O		800 nm ≥ λ ≥ 420 nm (500 W Xe light source)	[22]
Co-FPy-CON (Ir[dF(CF_3)ppy]$_2$(dtBpy))PF_6	1681 (CO)	TEOA	76%(CO)	λ > 420 nm (300 W Xe light source)	[23]
Co/CTF-1 $[Ru(Bpy)_3]Cl_2$	50 (CO)	TEOA	-	λ > 420 nm (300 W Xe light source)	[24]
SnS_2/S-CTFs	123.6(CO) 43.4 (CH4)	TEOA	-	λ > 420 nm (300 W Xe light source)	[25]
Re-CTF-py	353.05(CO)	TEOA		200 ~ 1100 nm (300 W	[26]

				Xe light source)	
CTF-TPN	330.3 (CO)	TEOA		λ > 420 nm (300 W Xe light source)	[27]
NCTF-1	11.48 (CH_4)	triethylamine (TEA)	85.42% (CH_4)	visible light (300 W Xe light source)	[28]
$ZnFe_2O_4$/FeP-CTFs $[Ru(Bpy)_3]Cl_2$	178 (CH_4)	TEOA		λ > 420 nm (300 W Xe light source)	[29]
Pt-SA/CTF-1	4.5 (CH_4)	triethylamine (TEA)	76.6%(CH_4)	λ > 420 nm (300 W Xe light source)	[30]
TiO_2@CTF-Py	43.34 (CO)	H_2O	98.3% (CO)	λ > 320 nm (300 W Xe light source)	[31]
$Ni(OH)_2$/CTF-1 $[Ru(Bpy)_3]Cl_2$	38.66 (CO)	TEOA	-	λ > 420 nm (300 W Xe light source)	[32]
CTF-BP	7.68 (CH_4)	TEOA	-	λ > 420 nm	[33]
CPB/CTF-1-Ni	86.5 (CO)	EA	-	λ > 400 nm (300 W	[34]

				Xe light source)	
$CuCo_2O_4$/CTF-1 $[Ru(Bpy)_3]Cl_2$	14.9 (CO)	TEOA	-	$\lambda > 420$ nm (300 W Xe light source)	[35]
Fe_2O_3@Por-CTF-10/$Ru(Bpy)_3Cl_2$	400(CO)	TEOA	93% (CO)	$\lambda > 420$ nm (300 W Xe light source)	[36]

[1] Wang, K., Yang, L., Guo, L., Cheng, G., Zhang, C., Jin, S., Tan, B., Cooper, A., I. Covalent Triazine Frameworks via a Low-Temperature Polycondensation Approach. *Angew. Chem. Int. Ed*., **2017**, 56 (45): 14149-14153.

[2] Liu, M., Huang, Q., Wang, S., Li, Z., Li, B., Jin, S., Tan, B. Crystalline Covalent Triazine Frameworks by In Situ Oxidation of Alcohols to Aldehyde Monomers. *Angew. Chem. Int. Ed*., **2018**, 57 (37): 11968-11972.

[3] Liu, M., Jiang, K., Ding, X., Wang, S., Zhang, C., Liu, J., Zhan, Z, Cheng, G., Li, B., Chen, H., Jin, S., Tan, B. Controlling Monomer Feeding Rate to Achieve Highly Crystalline Covalent Triazine Frameworks. *Adv. Mater.*, **2019**, 31 (19): 1807865.

[4] Zhang, S., Cheng, G., Guo, L., Wang, N., Tan, B., Jin, S. Strong-Base-Assisted Synthesis of a Crystalline Covalent Triazine Framework with High Hydrophilicity via Benzylamine Monomer for Photocatalytic Water Splitting. *Angew. Chem. Int. Ed*., **2020**, 59 (15): 6007-6014.

[5] Guo, L., Wang, X., Zhan, Z., Zhao, Y., Chen, L., Liu, T., Tan, B., Jin, S. Crystallization of Covalent Triazine Frameworks via a Heterogeneous Nucleation Approach for Efficient Photocatalytic Applications. *Chem. Mater.*, **2021**, 33 (6): 1994-2003.

[6] Wang, X., Zhang, S., Li, X., Zhan, Z., Tan, B., Lang, X., Jin, S. Two-Dimensional Crystalline Covalent Triazine Frameworks via Dual Modulator Control for Efficient Photocatalytic Oxidation of Sulfides. *J. Mater. Chem. A*, **2021**, 9 (30): 16405-16410.

[7] Yang, Z., Chen, H., Wang, S., Guo, W., Wang, T., Suo, X., Jiang, D., Zhu, X., Popovs, I., Dai, S. Transformation Strategy for Highly Crystalline Covalent Triazine Frameworks: from Staggered AB to Eclipsed AA Stacking. *J. Am. Chem. Soc.*, **2020**, 142 (15): 6856-6860.

[8] Sun, T., Liang, Y., Xu, Y. Rapid, Ordered Polymerization of Crystalline Semiconducting Covalent Triazine Frameworks. *Angew. Chem. Int. Ed*., **2022**, 61 (4): e202116875.

[9] Lan, Z. A., Wu, M., Fang, Z., Zhang, Y., Chen, X., Zhang, G., Wang, X., *Angew.*

Chem. Int. Ed., **2022**, 61 (4): e202201482.
[10] Bi, S., Yang, C., Zhang, W., Xu, J., Liu, L., Wu, D., Wang, X., Han, Y., Liang, Q., Zhang, F. Two-Dimensional Semiconducting Covalent Organic Frameworks via Condensation at Arylmethyl Carbon Atoms. *Nat. Commun*., **2019**, 10 (1): 2467.
[11] Xu, J., He, Y., Bi, S., Wang, M., Yang, P., Wu, D., Wang, J., Zhang, F. An Olefin-Linked Covalent Organic Framework as a Flexible Thin-Film Electrode for a High-Performance Micro-Supercapacitor. *Angew. Chem. Int. Ed*., **2019**, 58 (35): 12065-12069.
[12] Wei, S., Zhang, F., Zhang, W., Qiang, P., Yu, K., Fu, X., Wu, D., Bi, S., Zhang, F. Semiconducting 2D Triazine-Cored Covalent Organic Frameworks with Unsubstituted Olefin Linkages. *J. Am. Chem. Soc.*, **2019**, 141 (36): 14272-14279.
[13] Jadhav, T., Fang, Y., Patterson, W., Liu, C., Hamzehpoor, E., Perepichka, D., F. 2D Poly(arylene vinylene) Covalent Organic Frameworks via Aldol Condensation of Trimethyltriazine. *Angew. Chem. Int. Ed.*, **2019**, 58 (39): 13753-13757.
[14] Bi, S., Thiruvengadam, P., Wei, S., Zhang, W., Zhang, F., Gao, L., Xu, J., Wu, D., Chen, J., Zhang, F. Vinylene-Bridged Two-Dimensional Covalent Organic Frameworks via Knoevenagel Condensation of Tricyanomesitylene. *J. Am. Chem. Soc.*, **2020**, 142 (27): 11893-11900.
[15]. Ravel, B. & Newville, M. ATHENA, ARTEMIS, HEPHAESTUS: data analysis for X-ray absorption spectroscopy using IFEFFIT. *J. Synchrotron Radiat.* **12**, 537-541 (2005).
[16]. Koningsberger, D. C. & Prins, R. X-ray Absorption: Principles, Applications, Techniques of EXAFS, SEXAFS, and XANES (eds Koningsberger, D. C. & Prins, R.) Vol. 92 (Wiley, 1988).
[17]. Rehr, J. J. & Albers, R. C. Theoretical approaches to X-ray absorption fine structure. *Rev. Mod. Phys.***72**, 621-654 (2000).
[18] Lu, M., Li, Q., Liu, J., Zhang, F., Zhang, L., Wang, J., Kang, Z., Lan, Y. Installing Earth-Abundant Metal Active Centers to Covalent Organic Frameworks for Efficient Heterogeneous Photocatalytic CO_2 Reduction. *Appl. Catal., B*, **2019**, 254: 624-633.
[19] Fu, Z., Wang, X., Gardner, A., M., Wang, X., Chong, S., Y., Neri, G., Cowan, A., J., Liu, L., Li, X., Vogel, A., Clowes, R., Bilton, M., Chen, L., Sprick, R., S. Cooper, A., I. A Stable Covalent Organic Framework for Photocatalytic Carbon Dioxide Reduction. *Chem. Sci.*, **2020**, 11 (2): 543-550.
[20] Zhong, W., Sa, R., Li, L., He, Y., Li, L., Bi, J., Zhuang, Z., Yu, Y., Zou, Z. A Covalent Organic Framework Bearing Single Ni Sites as a Synergistic Photocatalyst for Selective Photoreduction of CO_2 to CO. *J. Am. Chem. Soc.*, **2019**, 141 (18): 7615-7621.
[21] Lu, M., Liu, J., Li, Q., Zhang, M., Liu, M., Wang, J., Yuan, D., Lan, Y. Rational Design of Crystalline Covalent Organic Frameworks for Efficient CO_2 Photoreduction with H_2O. *Angew. Chem. Int. Ed.*, **2019**, 58 (36): 12392-12397.
[22] Fu, Y., Zhu, X., Huang, L., Zhang, X., Zhang, F., Zhu, W. Azine-Based Covalent Organic Frameworks as Metal-Free Visible Light Photocatalysts for CO_2 Reduction with H_2O. *Appl. Catal., B*, **2018**, 239: 46-51.

[23] Wang, X., Fu, Z., Zheng, L., Zhao, C., Wang, X., Chong, S., McBride, F., Raval, R., Bilton, M., Liu, L., Wu, X., Chen, L., Sprick, R., S., Cooper, A., I. Covalent Organic Framework Nanosheets Embedding Single Cobalt Sites for Photocatalytic Reduction of Carbon Dioxide. *Chem. Mater.*, **2020**, 32 (21): 9107-9114.
[24] Bi, J., Xu, B., Sun, L., Huang, H., Fang, S., Li, L., Wu, L. A Cobalt-Modified Covalent Triazine-Based Framework as an Efficient Cocatalyst for Visible-Light-Driven Photocatalytic CO_2 Reduction. *Chempluschem*, **2019**, 84 (8): 1149-1154.
[25] Guo, S., Yang, P., Zhao, Y., Yu, X., Wu, Y., Zhang, H., Yu, B., Han, B., George, M. W., Liu, Z. Direct Z-Scheme Heterojunction of SnS_2/Sulfur-Bridged Covalent Triazine Frameworks for Visible-Light-Driven CO_2 Photoreduction. *Chemsuschem*, **2020**, 13 (23): 6278-6283.
[26] Xu, R., Wang, X., Zhao, H., Lin, H., Huang, Y., Cao, R. Rhenium-modified Porous Covalent Triazine Framework for Highly Efficient Photocatalytic Carbon Dioxide Reduction in a Solid-Gas System. *Catal. Sci. Technol.*, **2018**, 8 (8): 2224-2230.
[27] He, Y., Chen, X., Huang, C., Li, L., Yang, C., Yu, Y. Encapsulation of Co Single Sites in Covalent Triazine Frameworks for Photocatalytic Production of Syngas. *Chin. J. Catal.*, **2021**, 42 (1): 123-130.
[28] Niu, Q., Cheng, Z., Chen, Q., Huang, G., Lin, J., Bi, J., Wu, L. Constructing Nitrogen Self-Doped Covalent Triazine-Based Frameworks for Visible-Light-Driven Photocatalytic Conversion of CO_2 into CH_4. *ACS Sustainable Chem. Eng.*, **2021**, 9 (3): 1333-1340.
[29] Yan, Y., Fang, Q., Pan, J., Yang, J., Zhang, L., Zhang, W., Zhuang, G., Zhong, X., Deng, S., Wang, J. Efficient Photocatalytic Reduction of CO_2 Using Fe-based Covalent Triazine Frameworks Decorated with in Situ Grown $ZnFe_2O_4$ Nanoparticles., *Chem. Eng. J.*, **2021**, 408: 127358.
[30] Huang, G., Niu, Q., Zhang, J., Huang, H., Chen, Q., Bi, J., Wu, L. Platinum Single-Atoms Anchored Covalent Triazine Framework for Efficient Photoreduction of CO_2 to CH_4. *Chem. Eng. J.*, **2022**, 427: 131018.
[31] Xu, Z., Cui, Y., Young, D., Wang, J., Li, H., Bian, G., Li, H. Combination of Co2+-immobilized Covalent Triazine Framework and TiO_2 By Covalent Bonds to Enhance Photoreduction of CO_2 to CO with H_2O. *J. CO_2 Util.*, **2021**, 49: 101561.
[32] Zhao, T., Niu, Q., Huang, G., Chen, Q., Gao, Y., Bi, J., Wu, L. Rational Construction Of $Ni(OH)_2$ Nanoparticles on Covalent Triazine-Based Framework for Artificial CO_2 Reduction. *J. Colloid Interface Sci.*, **2021**, 602: 23-31.
[33] Li, J., Liu, P., Huang, H., Li, Y., Tang, Y., Mei, D., Zhong, C. Metal-Free 2D/2D Black Phosphorus and Covalent Triazine Framework Heterostructure for CO_2 Photoreduction. *ACS Sustainable Chem. Eng.*, **2020**, 8 (13): 5175-5183.
[34] Zhong, H., Hong, Z., Yang, C., Li, L., Xu, Y., Wang, X., Wang, R. A Covalent Triazine-Based Framework Consisting of Donor-Acceptor Dyads for Visible-Light-Driven Photocatalytic CO_2 Reduction. *Chemsuschem*, **2019**, 12 (19): 4493-4499.
[35] Lin, G., Sun, L., Huang, G., Chen, Q., Fang, S., Bi, J., Wu, L. Direct Z-scheme Copper Cobaltite/Covalent Triazine-Based Framework Heterojunction for Efficient Photocatalytic CO_2 Reduction under Visible Light. *Sustainable Energy Fuels*, **2021**, 5

(3): 732-739.
[36] Zhang, S., Wang, S., Guo, L., Chen, H., Tan, B., Jin, S. An Artificial Photosynthesis System Comprising a Covalent Triazine Framework as an Electron Relay Facilitator for Photochemical Carbon Dioxide Reduction. *J. Mater. Chem. C*, **2020**, 8 (1): 192-200.